Front. Phys. 11(5), 115207 (2016)
DOI 10.1007/s11467-016-0619-9

RESEARCH ARTICLE

In situ analysis of magnesium alloy using a standoff and double-pulse laser-induced breakdown spectroscopy system

Yong Xin (辛勇)[1,2], **Lan-Xiang Sun** (孙兰香)[1,†], **Zhi-Jia Yang** (杨志家)[1], **Peng Zeng** (曾鹏)[1], **Zhi-Bo Cong** (丛智博)[1], **Li-Feng Qi** (齐立峰)[1]

[1] *Key Laboratory of Networked Control Systems, Shenyang Institute of Automation, Chinese Academy of Sciences, Shenyang 110016, China*
[2] *University of Chinese Academy of Sciences, Beijing 100049, China*
Corresponding author. E-mail: †sunlanxiang@sia.cn
Received May 20, 2016; accepted July 20, 2016

To monitor the components of molten magnesium alloy during the smelting process in real time and online, we designed a standoff double-pulse laser-induced breakdown spectroscopy (LIBS) analysis system that can perform focusing, collecting and imaging of long-range samples. First, we tested the system on solid standard magnesium alloy samples in the laboratory to establish a basis for the online monitoring of the components of molten magnesium alloy in the future. The experimental results show that the diameters of the focus spots are approximately 1 mm at a range of 3 m, the ablation depth of the double-pulse mode is much deeper than that of the single-pulse mode, the optimum interpulse delay of the double pulse is inconsistent at different ranges, and the spectral intensity decays rapidly as the range increases. In addition, the enhancement effect of the double pulse at 1.89 m is greater than that at 2.97 m, the maximum enhancement is 7.1-fold for the Y(I)550.35-nm line at 1.89 m, and the calibration results at 1.89 m are better than those at 2.97 m. At 1.89 m, the determination coefficients (R^2) of the calibration curves are approximately 99% for Y, Pr, and Zr; the relative standard deviations (RSDs) are less than 10% for Y, Pr, and Zr; the root mean square errors (RMSEs) are less than 0.037% for Pr and Zr; the limits of detection (LODs) are less than 1000 ppm for Y, Pr, and Zr; and the LODs of Y, Pr, and Zr at 2.97 m are higher than those at 1.89 m. Additionally, we tested the system on molten magnesium alloy in a magnesium alloy plant. The calibration results of the liquid magnesium alloy are not as favorable as those of the sampling solid magnesium alloys. In particular, the RSDs of the liquid magnesium alloy are approximately 20% for Pr and La. However, with future improvements in the experimental conditions, the developed system is promising for the in situ analysis of molten magnesium alloy.

Keywords laser-induced breakdown spectroscopy, standoff, double-pulse, online, magnesium alloy

PACS numbers 52.25.Kn, 52.38.Mf, 42.62.Cf, 42.62.Fi

1 Introduction

Magnesium alloys, which are known as green engineering materials for the 21st century, are the lightest metal structural materials used in practical applications. Adding rare-earth elements to a magnesium alloy can greatly improve the performance of the alloy so that it has wider application in the aerospace, automotive, electronics, military, and other fields [1]. At present, the elemental analysis of magnesium alloy concentrations is mainly performed offline, which can take from a few minutes to a few days. Offline analysis severely limits the bulk production of magnesium alloys and the rapid development of new types of magnesium alloys.

Laser-induced breakdown spectroscopy (LIBS) technology [2–4] uses a focused laser to ablate the surface of an object to generate plasma. Then, qualitative and

*Special Topic: The 1st Asian Symposium on Laser-induced Breakdown Spectroscopy (Eds. Xiao-Yan Zeng, Zhe Wang & Yoshihiro Deguchi).

quantitative analyses of the measured objects can be performed by collecting and analyzing the plasma spectra. Because LIBS technology has advantages such as simultaneous and fast multi-element analysis, no sample preparation requirements, and the ability to measure all sample types, it has received the attention of scholars in many fields [5–21].

Because of the lack of the need for sample preparation and the speed of acquisition, thereby allowing online measurement, many scholars have applied LIBS technology to online analysis in the metallurgical industry. Carlhoff and Kirchhoff [22] were the first to apply LIBS to the in situ analysis of molten steel in a converter. Noll *et al.* [23, 24] applied LIBS to guide the smelting process of steel, and performed composition control and quality monitoring of molten steel. Energy Research Company, funded by the US Department of Energy, developed a system that can monitor the composition of molten aluminum alloy in real time [25]. Hubmer *et al.* [26] proposed a method for analyzing liquid high-alloy steel using a fiber-optic cable to carry the signal over a distance of approximately 10 m. Palanco *et al.* [27] designed a remote open-path LIBS system and successfully monitored the concentrations of Cr and Ni in liquid steel. Victor [28] successfully adapted a Newtonian telescope to continuously monitor changes in Si and Mn concentrations in blast furnace runners. Dong *et al.* [29] introduced recent progress on the application of LIBS to metallurgical online analysis in China. Sun *et al.* [30, 31] used LIBS technology to monitor the composition of liquid steel online. Chen *et al.* [32] also reported on the real-time quantitative analysis of multiple elements in molten steel by LIBS. Pořízka *et al.* [33] reported on the potential use of the LIBS technique for the direct investigation of Mg corrosion. However, online analysis of the composition of molten magnesium alloy by LIBS has not yet been reported.

In recent years, double-pulse LIBS technology and remote LIBS technology have received much attention from researchers. Using a double pulse separated by a short delay time (several microseconds) can result in a lower LOD and significant enhancements of emission line intensity, as well as significantly improved signal-to-noise ratios (SNR) [34, 35]. Remote LIBS technology is very suitable for application in the fields of metallurgy, archaeology, and space engineering [27, 31, 36–38].

We combined double-pulse LIBS and remote LIBS to develop a standoff double-pulse coaxial LIBS analysis system. In this study, we tested the system on solid standard magnesium alloy samples in the laboratory and liquid magnesium alloy in a magnesium alloy plant.

2 Experimental

2.1 Experiment system

A schematic diagram of the experimental system is shown in Fig. 1. First, two Nd:YAG lasers (Beamtech Dawa-200 with a wavelength of 1064 nm, pulse energy of 200 mJ, pulse width of 8–10 ns, repetition frequency of 10 Hz, and spot diameter of 7 mm) were combined. The combined laser beams were reflected into a laser beam expander (magnification of 3.3×) by mirrors 1 and 2. The laser beams were then reflected to a dichroic mirror by mirror 3, expanded a second time (magnification of 4.8×) by a telescope system, and then focused on the surface of samples at a long range to stimulate the sam-

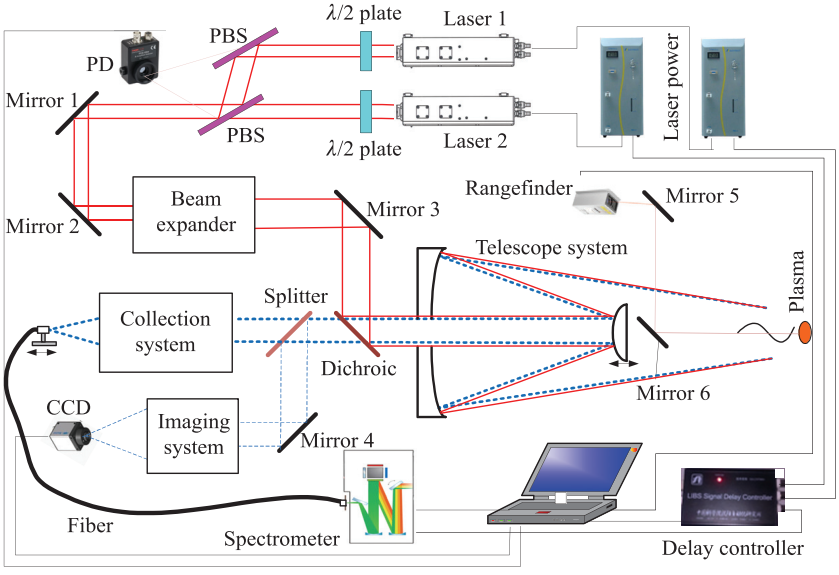

Fig. 1 Schematic diagram of the experimental system.

ples and generate the plasma. The plasma emission light was collected using the telescope system, passed through the dichroic mirror and beam splitter, and then coupled into the fiber using the collection system. Finally, the emission light was transmitted via the fiber to the spectrometer (Ocean Optics HR2000 with a spectral range of 200–600 nm and resolution of approximately 0.1 nm).

A portion of the visible light (approximately 10%) was separated by a beam splitter and reflected to the imaging system by mirror 4, which can display remote laser focal position information in real time. The delay time between the two lasers and the gate delay time of the spectrometer were set and controlled by a multichannel delay controller designed by our team. A laser rangefinder was used to measure the distance between the rangefinder and samples using mirrors 5 and 6. Thus, the telescope system can automatically adjust the distance of the primary mirror to the secondary mirror to achieve the best laser focusing and spectra collection performance.

Compared with one of our previously developed systems [31], this system only needs to change the distance between the primary mirror and the secondary mirror to achieve the automatic simultaneous optimization of the laser focusing and spectra collection based on the range information measured by a rangefinder. However, because of the limitation of the coating on the dichroic mirror used in the system, the collection efficiency is low in the ultraviolet band, and some of the bands are completely unable to be detected.

2.2 Experimental conditions and standard samples for laboratory tests

Because of the influence of bremsstrahlung and free-bound electronic recombination continuum radiation, at the beginning of the plasma generation, the emitted spectrum has a low SNR, and changing the delay time between the pulses and the spectrometer could efficiently improve the SNR. In the experiment, the spectrometer gate delay time after the second laser pulse was set to 1 μs, the pulse energy of both lasers was set to 100 mJ, the mean irradiance of the sample was greater than 1 GW/cm^2, and the test distances from the lasers to the sample were 1.89 m and 2.97 m, respectively.

To eliminate the effect of surface contamination, the first 20 spectra were not collected before each test. Subsequently, 200 spectra were acquired and averaged into a single spectrum to reduce the spectral fluctuations that are caused by factors such as the experimental environment and the uneven surfaces of the samples.

The samples were five rare earth magnesium alloy types, which were provided by the Institute of Metal Research, Chinese Academy of Sciences. The compositions of the samples are listed in Table 1.

Table 1 Compositions of the rare earth magnesium alloy samples.

Sample No.	Concentration (%)				
	Y	La	Pr	Zr	Mg
1	1.44	1.06	0.11	—	97.39
2	2.22	2.46	0.29	0.01	95.02
3	1.41	4.27	0.52	0.13	93.67
4	2.10	6.00	0.77	0.44	90.69
5	2.70	8.05	1.04	0.76	87.45

2.3 In situ analysis of liquid magnesium alloy

After the laboratory testing, the LIBS system was transferred to a magnesium alloy plant of the Institute of Metal Research, Chinese Academy of Sciences, for application testing. Figure 2 shows photos of the test site. A stainless steel tube (with a length of 2.2 m and a distance from the laser to the sample of approximately 3 m), connected to the integrated optical box by a flange, was used to transmit the laser beam and the plasma emissions. Argon was blown through the steel tube to disperse the smoke and slag on the melt surface. Initially, we planned to use a refractory lance that was joined at the tip of the steel tube to be immersed into the molten magnesium alloy to pass through the surface slag layer, as shown in Fig. 2(a). Magnesium alloy, however, is prone to burn during the insertion process, and thus produces a large amount of smoke. Therefore, we used the method of blowing gas on the melt surface to disperse the slag from the region in focus, as shown in Fig. 2(b).

In the experiment, we used two rare earth elements, La and Pr. First, 17 kg of pure magnesium was melted in the magnesium alloy furnace, and then the lanthanum-rich rare earth (45% La and 11% Pr) was added. When the lanthanum-rich rare earth was completely melted and

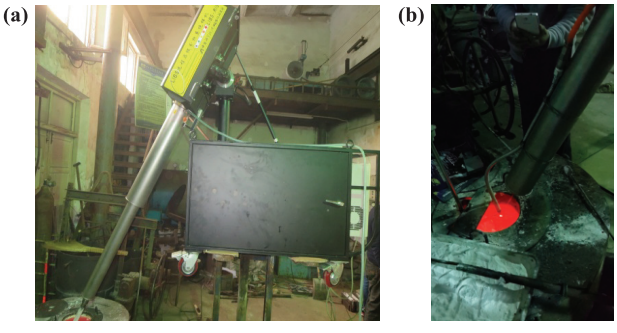

Fig. 2 Photos of the test site in a magnesium alloy plant. **(a)** The refractory lance tip immersed into the molten magnesium alloy. **(b)** Blowing gas on the melt surface via a flexible steel tube.

Table 2 Compositions of liquid magnesium alloy samples.

Sample No.	Concentration (%)	
	La	Pr
1	0.09	0.01
2	1.29	0.093
3	2.81	0.18
4	4.16	0.27

mixed with the magnesium, the argon-purged steel tube was positioned approximately 1 cm above the surface of the liquid magnesium alloy for testing. When adequate data had been obtained, the system was elevated to a certain height to wait for the next test, and then the melt was sampled for a laboratory analysis. The tests were conducted on four groups of samples, in which the amounts of the lanthanum-rich rare earth added were 17 g, 325 g, 361 g, and 382 g.

The solid samples from the magnesium alloy furnace were sent to a laboratory for offline analysis by ICP-OES, and the given concentrations of the elements are shown in Table 2.

3 Results and discussion

3.1 Remote imaging and remote focusing

The imaging system can remotely image objects at different distances. Figure 3 shows the images of the focus spots on the first magnesium alloy sample at different distances. The imaging system can be used to rapidly observe the morphology of an object at a long range or direct the laser focus to the position expected.

For a Gaussian beam, the minimum achievable spot radius r satisfies the following equation [39]:

$$r = \frac{2\lambda R}{\pi D} M^2, \tag{1}$$

where λ is the laser wavelength, R is the focusing range, D is the diameter of the laser beam before focusing, and M^2 is the laser beam quality factor.

According to formula (1), the minimum spot radius r is proportional to the focusing range R and is inversely proportional to the diameter of the laser beam D. To reduce the radius of the focus spot, the laser beam should be expanded, which will further reduce the divergence angle of the laser beam.

The focus spot sizes at different ranges are shown in Fig. 4. As observed from Fig. 4, the diameters of the focus spots are approximately 1 mm at a range of 3 m, and the spot sizes become larger with increasing distance, which is consistent with formula (1). However, the diameter of the laser beam D varies with the focusing range of the system. When the range is longer, the diameter of laser beam D is larger. Thus, the laser beam spot radius r is actually not proportional to the focusing range R.

Figure 5 shows a comparison of the focus spots of the single-pulse (SP) mode and the double-pulse (DP) mode at 2.35 m. From Fig. 5, the ablation depth of the double-pulse mode is much deeper than that of the single-pulse mode, indicating that the sampled mass of melting and evaporation is much larger in the double-pulse mode. After the first laser pulse was shot on the sample, the sample surface was softened and heated. When the second laser beam was shot on the softened and heated sample surface, the sample was much more easily stripped, and thus the depth of ablation is deeper in the double-pulse

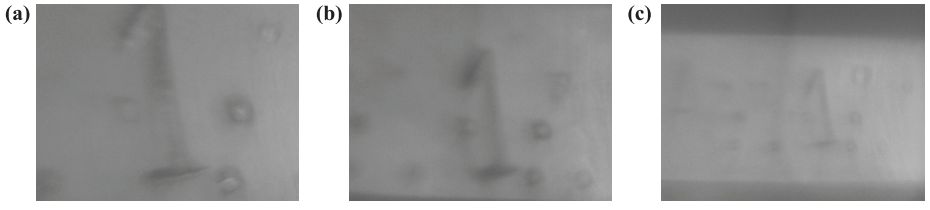

Fig. 3 Remote imaging of the focus spots on the first magnesium alloy sample at distances of 1.89 m **(a)**, 2.97 m **(b)** and 4.44 m **(c)**. The length of the number 1 is approximately 9 mm in the figures shown.

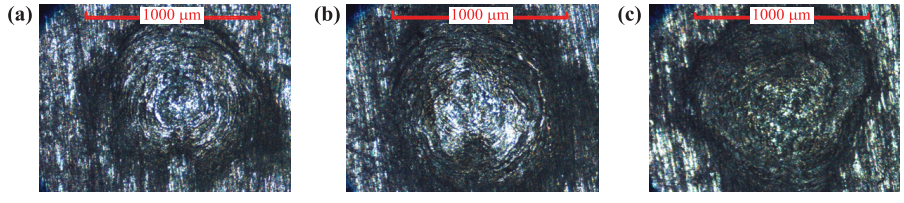

Fig. 4 The focus spot at distances of 1.89 m **(a)**, 2.97 m **(b)** and 4.44 m **(c)**.

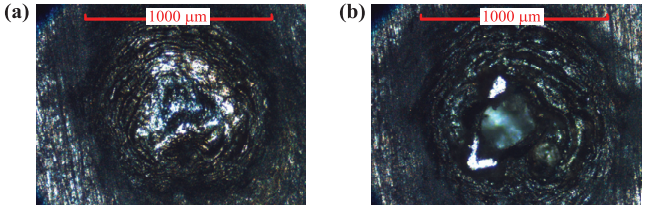

Fig. 5 Comparison of the focus spots of the single-pulse mode **(a)** and double-pulse mode **(b)** at 2.35 m.

mode [40]. This is consistent with the enhancement effect of double-pulse LIBS that was observed in the following experiments.

3.2 Interpulse delay between the two laser pulses

The interpulse delay between the two laser pulses is an important factor that affects the signal intensity of double-pulse LIBS [34, 35]. We altered the interpulse delay between the two laser pulses and determined the relationship between the spectral intensity and the interpulse delay. Figure 6 shows the relationship between the spectral intensity and interpulse delay at different distances. When the interpulse delay is 8 μs, the intensity of La, Pr, Y, and Zr is strongest at 1.89 m. When the interpulse delay is 10 μs, the spectral intensity of most of the elements (with the exception of Y, which is strongest with a delay of 6 μs) is strongest at 2.97 m. These results show that the optimum interpulse delay is different at different focusing ranges. This is because the plasma conditions are different at different ranges. Thus, in the experiment, we needed to find the optimum interpulse delay at different ranges.

3.3 Relationship between spectral intensity and focusing range

To collect the LIBS signal, the intensity of the signal is proportional to the solid angle and inversely proportional to the square of the focusing range under identical plasma conditions [38]:

$$I_{LIBS} \propto n_D = n_E \frac{\Omega}{4\pi} = \frac{A}{4\pi R^2}, \tag{2}$$

where n_D is the number of detected photons for a given wavelength, n_E is the number of emitted photons of the same wavelength, Ω is the solid angle of collection, R is the focusing range, and A is the area illuminated in the primary mirror.

Figure 7 shows the relationship between the intensity of the Mg (I) 277.98-nm line and the focusing range. However, the curve in Fig. 7 does not fit to an inverse square function, which indicates that the plasma conditions vary with the focusing range. Furthermore, as mentioned above, the remote focus spot increases as the focusing range increases, and thus the peak power of the laser decreases with the focusing range. Therefore, the LIBS signal is weaker at a long range.

3.4 Enhancement effect of double-pulse LIBS

To compare the single-pulse and double-pulse spectra under the same experimental conditions, we set the laser pulse energy to 80 mJ in the single-pulse mode and 40 mJ for each of the pulses in the double-pulse mode.

Figure 8 shows the enhancement effect of double-pulse LIBS at 1.89 m, which indicates that the double-pulse LIBS signal is significantly higher than the single-pulse LIBS signal. Because the first laser beam changes the state of the sample surface and increases its temperature, the second laser beam then passes through the plasma and interacts with the high-temperature sample surface, thus stimulating more particles in the double-pulse mode [31]. These results are consistent with the abovementioned phenomenon of the ablation depth.

Table 3 shows the enhancement effect of the double-pulse LIBS at 1.89 m and 2.97 m. At 1.89 m, using double-pulse LIBS results in a 7.1-fold enhancement in

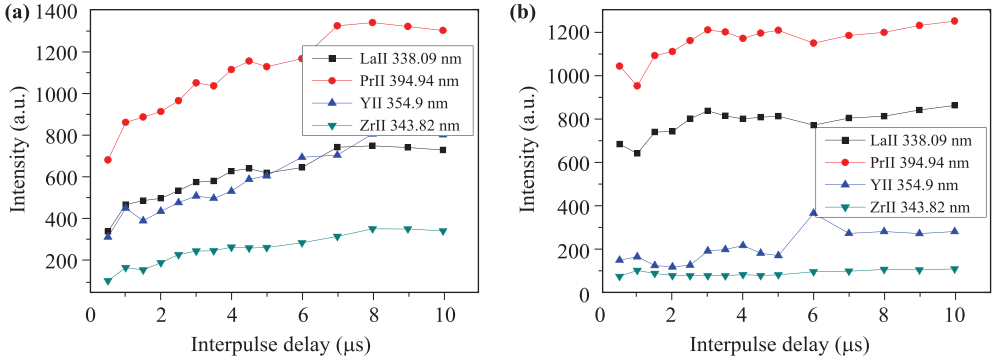

Fig. 6 Variation of the spectral intensity with the interpulse delay between the two laser pulses at distances of 1.89 m **(a)** and 2.97 m **(b)**.

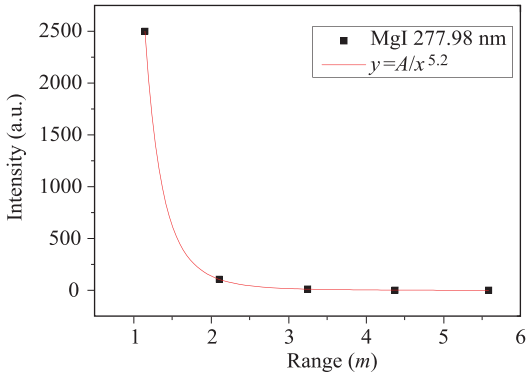

Fig. 7 Variation of the intensity of the Mg (I) 277.98 nm line with the focusing range.

the spectral intensity of the Y (I) 550.35-nm line. As seen in Table 3, the enhancement effect is weaker at longer range than shorter range because the two laser pulses were not well combined for the long range. As Fig. 9 shows, the focus spot is not symmetric at the long range, and the depth of ablation is shallower than that for the short range. Therefore, the enhancement effect for the long range is weaker.

3.5 Calibration results of solid standard magnesium alloys

The internal standard method was used to calibrate the solid standard magnesium alloy samples at 2.97 m and 1.89 m. The analytical lines and reference lines for the different elements are Y (II) 354.9 nm [Mg (I) 332.99 nm], Pr (II) 395.67 nm [Mg (I) 332.99 nm], and Zr (II) 349.62 nm [Mg (I) 309.1 nm]. Figure 10 shows the calibration curves of the different elements at 1.89 m, and Table 4 shows calibration results of the different elements at different focusing ranges. As seen in Fig. 10 and Table 4, the calibration results are better at 1.89 m: R^2 values are approximately 99% for Y, Pr, and Zr; RSDs are less than 10% for Y, Pr, and Zr; RMSEs for Pr and Zr are less than 0.037%; and LODs are less than 1000 ppm for Y, Pr, and Zr.

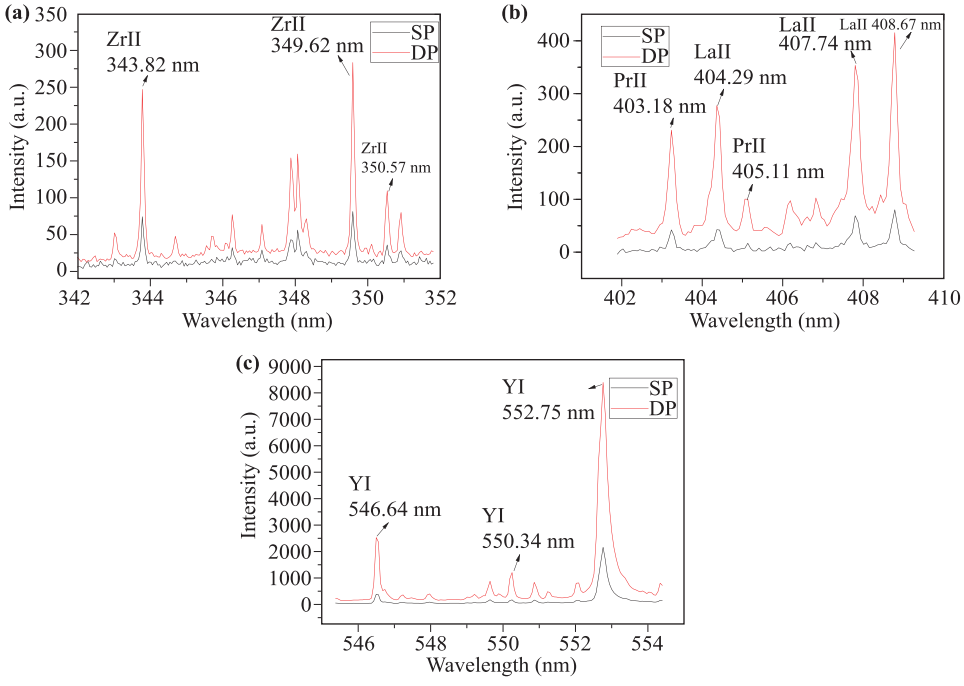

Fig. 8 Enhancement effect for different elements using double-pulse LIBS at 1.89 m. The elements shown are Zr **(a)**, La and Pr **(b)** and Y **(c)**.

Table 3 Enhancement effect of double-pulse LIBS at different focusing ranges.

Range	Wavelength (nm)										
	Y			La			Pr		Zr		
	546.64	550.34	552.75	404.29	407.74	408.67	403.18	405.11	343.82	349.62	350.57
1.89 m	6.7	7.1	3.9	6.5	5.1	6.0	5.5	5.9	3.3	3.5	3.1
2.97 m	4.0	3.7	2.1	3.8	2.6	3.2	3.2	–	1.8	1.6	1.7

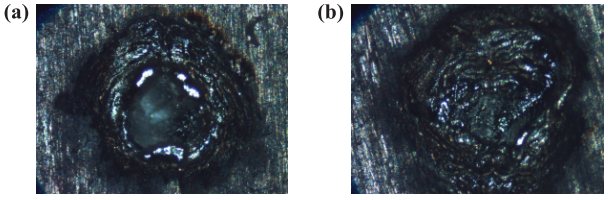

Fig. 9 Ablation morphology of the double pulse at distances of 1.89 m **(a)** and 2.97 m **(b)**.

The LOD is calculated as follows:

$$LOD = 3\sigma_B/S, \tag{3}$$

where σ_B is the standard deviation of the background, and S is the sensitivity of the analysis method, which is usually expressed as the slope of the calibration curve.

From Table 4, LODs for the long range are higher than those for the short range because the signals decay rapidly and the focus spot size increases for the long range.

3.6 Calibration results of liquid magnesium alloy samples

We analyzed the liquid and solid data, which were acquired during the liquid experiment and subsequent analysis of the sampled solid samples, respectively. The internal standard method was used to calibrate the elements La and Pr from the liquid and solid data. The analytical and respective reference lines for different elements are Pr (I) 566.85 nm [Mg (I) 571.11 nm] and La (II) 433.37 nm [Mg (I) 571.11 nm].

Table 4 Calibration results of different elements at different focusing ranges.

Parameters	Range	Pr	Zr	Y
R^2 (%)	1.89 m	99.0	99.5	98.6
	2.97 m	99.9	99.4	96.5
RSD (%)	1.89 m	6.26	9.84	6.85
	2.97 m	8.23	10.92	5.57
RMSE (%)	1.89 m	0.037	0.021	0.071
	2.97 m	0.005	0.023	0.113
LOD (ppm)	1.89 m	937	334	864
	2.97 m	1670	1054	1212

Figure 11 and Fig. 12 show calibration curves of the liquid and solid data. As seen in Fig. 11 and Fig. 12, the calibration results are good for the solid data but not good for the liquid data. In particular, The LODs of Pr and La in liquid data are approximately 2000 ppm, and the RSDs of Pr and La in liquid data are approximately 20%. Because the system was elevated to a certain height to wait for the next testing after a group of experiments was completed, the focus position is not very accurate

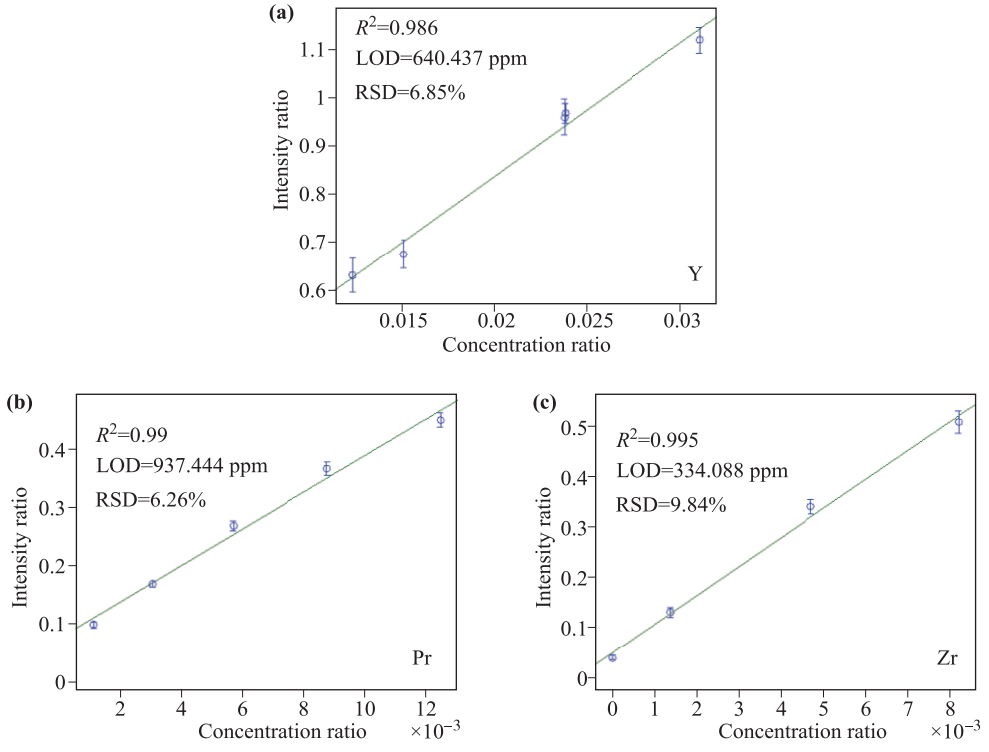

Fig. 10 Calibration curves of different elements at 1.89 m. The elements shown are Y **(a)**, Pr **(b)** and Zr **(c)**.

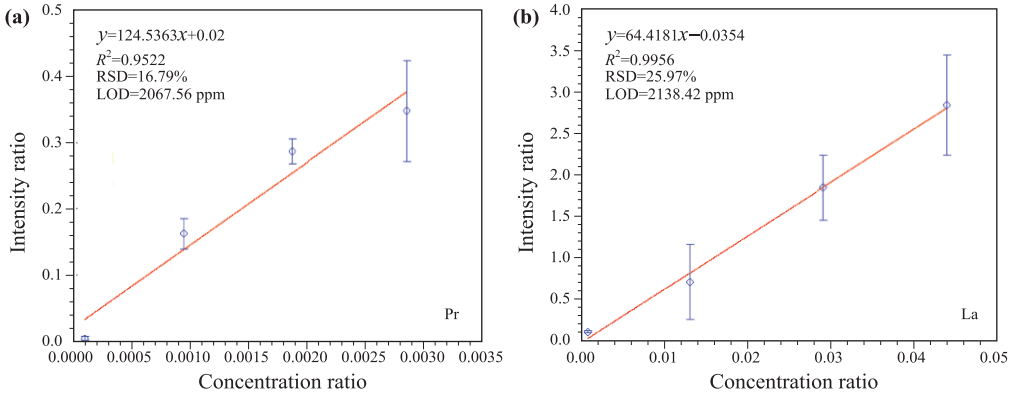

Fig. 11 Calibration curves of Pr **(a)** and La **(b)** for the liquid data.

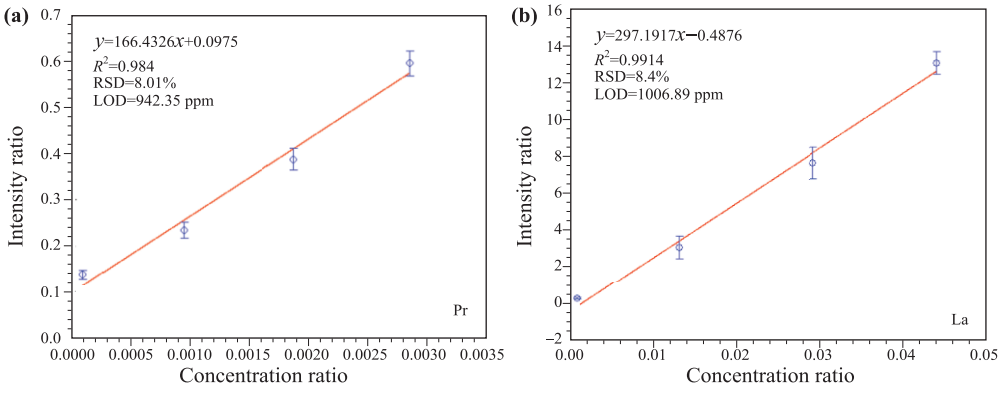

Fig. 12 Calibration curves of Pr **(a)** and La **(b)** for the solid data.

in each group of experiments. Additionally, the slag and smoke in the liquid magnesium alloy surface were not completely swept clean, which can create interference. In the future, further study is needed to position the focus more precisely and to reduce the interference of the surface slag and smoke in liquid magnesium alloy.

4 Conclusion

To monitor the components of molten magnesium alloy during the smelting process in real time and online, we combined double-pulse LIBS and remote LIBS to develop a standoff double-pulse coaxial LIBS analysis system.

We tested the system on solid standard magnesium alloy samples in the laboratory. The experimental results show the calibration results are good at 1.89 m: R^2 values are approximately 99% for Y, Pr, and Zr; RSDs are less than 10% for Y, Pr, and Zr; RMSEs for Pr and Zr are less than 0.037%; and LODs are less than 1000 ppm for Y, Pr, and Zr.

Additionally, we tested the system on molten magnesium alloy in a magnesium alloy plant. The calibration results of the liquid magnesium alloy are not as favorable as those of the sampling solid magnesium alloys. In particular, the RSDs of the liquid magnesium alloy are approximately 20% for Pr and La. However, with future improvements in experimental conditions, such as positioning the focus more precisely and reducing the interference of the surface slag and smoke in liquid magnesium alloy, the developed system is promising for the in situ analysis of molten magnesium alloy.

Acknowledgements This research work was financially supported by the National Natural Science Foundation China (Grant No. 61473279) and the National Key Research and Development Program of China (No. 2016YFF0102502).

References

1. W. J. Ding, Y. J. Wu, L. M. Peng, X. Q. Zeng, D. L. Lin, and B. Chen, Research and application development of advanced magnesium alloys, *Materials China* 29(8), 37 (2010)
2. A. W. Miziolek, V. Palleschi, and I. Schechter, Laser-induced Breakdown Spectroscopy (LIBS): Fundamentals and Applications, Cambridge: Cambridge University Press, 2006

3. D. A. Cremers and L. J. Radziemski, Handbook of Laser-induced Breakdown Spectroscopy, New York: John Wiley & Sons, Ltd, 2006
4. R. Noll, Laser-induced Breakdown Spectroscopy: Fundamentals and Applications, Berlin: Springer, 2011
5. D. W. Hahn and N. Omenetto, Laser-induced breakdown spectroscopy (LIBS), part II: Review of instrumental and methodological approaches to material analysis and applications to different fields, *Appl. Spectrosc.* 66(4), 347 (2012)
6. F. J. Fortes and J. J. Laserna, The development of fieldable laser-induced breakdown spectrometer: No limits on the horizon, *Spectrochim. Acta B At. Spectrosc.* 65(12), 975 (2010)
7. J. Kaiser, K. Novotný, M. Z. Martin, A. Hrdlicka, R. Malina, M. Hartl, V. Adam, and R. Kizek, Trace elemental analysis by laser-induced breakdown spectroscopy — Biological applications, *Surf. Sci. Rep.* 67(11-12), 233 (2012)
8. J. El Haddad, L. Canioni, and B. Bousquet, Good practices in LIBS analysis: Review and advices, *Spectrochim. Acta B At. Spectrosc.* 101, 171 (2014)
9. P. Pořízka, P. Prochazková, D. Prochazka, L. Sládková, J. Novotný, M. Petrilak, M. Brada, O. Samek, Z. Pilát, P. Zemánek, V. Adam, R. Kizek, K. Novotný, and J. Kaiser, Algal biomass analysis by laser-based analytical techniques—A review, *Sensors (Basel Switzerland)* 14(9), 17725 (2014)
10. A. K. Pathak, R. Kumar, V. K. Singh, R. Agrawal, S. Rai, and A. K. Rai, Assessment of LIBS for spectrochemical analysis: A review, *Appl. Spectrosc. Rev.* 47(1), 14 (2012)
11. Z. Wang, T. B. Yuan, Z. Y. Hou, W. D. Zhou, J. D. Lu, H. B. Ding, and X. Y. Zeng, Laser-induced breakdown spectroscopy in China, *Front. Phys.* 9(4), 419 (2014)
12. J. Yu and R. E. Zeng, Laser-induced plasma and laser-induced breakdown spectroscopy (LIBS) in China: The challenge and the opportunity, *Front. Phys.* 7(6), 647 (2012)
13. J. Vrenegor, R. Noll, and V. Sturm, Investigation of matrix effects in laser-induced breakdown spectroscopy plasmas of high-alloy steel for matrix and minor elements, *Spectrochim. Acta B At. Spectrosc.* 60(7–8), 1083 (2005)
14. M. A. Gondal and T. Hussain, Determination of poisonous metals in wastewater collected from paint manufacturing plant using laser-induced breakdown spectroscopy, *Talanta* 71(1), 73 (2007)
15. B. Hettinger, V. Hohreiter, M. Swingle, and D. W. Hahn, Laser-induced breakdown spectroscopy for ambient air particulate monitoring: correlation of total and speciated aerosol particle counts, *Appl. Spectrosc.* 60(3), 237 (2006)
16. F. Ferioli and S. G. Buckley, Measurements of hydrocarbons using laser-induced breakdown spectroscopy, *Combust. Flame* 144(3), 435 (2006)
17. T. B. Yuan, Z. Wang, S. L. Lui, Y. Fu, Z. Li, J. Liu, and W. Ni, Coal property analysis using laser-induced breakdown spectroscopy, *J. Anal. At. Spectrom.* 28(7), 1045 (2013)
18. L. B. Guo, Z. Q. Hao, M. Shen, W. Xiong, X. N. He, Z. Q. Xie, M. Gao, X. Y. Li, X. Y. Zeng, and Y. F. Lu, Accuracy improvement of quantitative analysis by spatial confinement in laser-induced breakdown spectroscopy, *Opt. Express* 21(15), 18188 (2013)
19. L. B. Guo, B. Y. Zhang, X. N. He, C. M. Li, Y. S. Zhou, T. Wu, J. B. Park, X. Y. Zeng, and Y. F. Lu, Optimally enhanced optical emission in laser-induced breakdown spectroscopy by combining spatial confinement and dual-pulse irradiation, *Opt. Express* 20(2), 1436 (2012)
20. W. D. Zhou, K. X. Li, Q. M. Shen, Q. Chen, and J. Long, Optical emission enhancement using laser ablation combined with fast pulse discharge, *Opt. Express* 18(3), 2573 (2010)
21. Y. Feng, J. J. Yang, J. M. Fan, G. X. Yao, X. H. Ji, X. Y. Zhang, X. F. Zheng, and Z. F. Cui, Investigation of laser-induced breakdown spectroscopy of a liquid jet, *Appl. Opt.* 49(13), C70 (2010)
22. C. Carlhoff and S. Kirchhoff, Laser-induced emission spectroscopy for on-line analysis of molten metal in a steel converter, *Laser und Optoelektronik* 23, 50 (1991)
23. R. Noll, H. Bette, A. Brysch, M. Kraushaar, I. Mönch, L. Peter, and V. Sturm, Laser-induced breakdown spectrometry applications for production control and quality assurance in the steel industry, *Spectrochim. Acta B At. Spectrosc.* 56(6), 637 (2001)
24. L. Peter, V. Sturm, and R. Noll, Liquid steel analysis with laser-induced breakdown spectrometry in the vacuum ultraviolet, *Appl. Opt.* 42(30), 6199 (2003)
25. R. D. Saro, A. Weisberg, and J. Craparo, in: Final Report Prepared for the U.S. Department of Energy Under Award Number DE-FC02-99CH10974, 2005
26. G. Hubmer, R. Kitzberger, and K. Morwald, Application of LIBS to the in-line process control of liquid high-alloy steel under pressure, *Anal. Bioanal. Chem.* 385(2), 219 (2006)
27. S. Palanco, S. Conesa, and J. J. Laserna, Analytical control of liquid steel in an induction melting furnace using a remote laser induced plasma spectrometer, *J. Anal. At. Spectrom.* 19(4), 462 (2004)
28. T. Victor, Future of the online control of molten metal, *Metall. Anal.* 33(4), 13 (2013)
29. F. Z. Dong, X. L. Chen, Q. Wang, L. X. Sun, H. B. Yu, Y. X. Liang, J. G. Wang, Z. B. Ni, Z. H. Du, Y. W. Ma, and J. D. Lu, Recent progress on the application of LIBS for metallurgical online analysis in China, *Front. Phys.* 7(6), 679 (2012)
30. L. X. Sun, H. B. Yu, and Y. Xin, Z. B. Cong and H. Y. Kong, On-line monitoring of molten steel compositions by laser-induced breakdown spectroscopy, *Chin. J. Lasers* 38(9), 0915002 (2011)

31. L. X. Sun, H. B. Yu, Z. B. Cong, Y. Xin, Y. Li, and L. F. Qi, In situ analysis of steel melt by double-pulse laser-induced breakdown spectroscopy with a Cassegrain telescope, *Spectrochim. Acta B At. Spectrosc.* 112, 40 (2015)
32. K. Chen, J. D. Lu, and J. Y. Li, Real-time quantitative analysis of multi-elements in liquid steel by LIBS, *Guangpuxue Yu Guangpu Fenxi* 31(3), 823 (2011)
33. P. Pořízka, I. Ročňáková, J. Klus, D. Prochazka, L. Sládková, P. Šperka, Z. Spotz, L. Čelko, K. Novotný, and J. Kaiser, Estimating the grade of Mg corrosion using laser-induced breakdown spectroscopy, *J. Anal. At. Spectrom.* 30(10), 2099 (2015)
34. F. Sorrentino, G. Carelli, F. Francesconi, M. Francesconi, P. Marsili, G. Cristoforetti, S. Legnaioli, V. Palleschi, and E. Tognoni, Fast analysis of complex metallic alloys by double-pulse time-integrated laser-induced breakdown spectroscopy, *Spectrochim. Acta B At. Spectrosc.* 64(10), 1068 (2009)
35. D. Stratis, K. Eland, and M. Angel, Dual-pulse LIBS using a pre-ablation spark for enhanced ablation and emission, *Appl. Spectrosc.* 54(9), 1270 (2000)
36. I. Gaona, P. Lucena, J. Moros, F. J. Fortes, S. Guirado, J. Serrano, and J. J. Laserna, Evaluating the use of standoff LIBS in architectural heritage: surveying the Cathedral of Málaga, *J. Anal. At. Spectrom.* 28(6), 810 (2013)
37. R. C. Wiens, S. Maurice, B. Barraclough, M. Saccoccio, W. C. Barkley, et al., The ChemCam instrument suite on the Mars Science Laboratory (MSL) rover: Body unit and combined system tests, *Space Sci. Rev.* 170, 167 (2012)
38. S. Palanco, C. Lo'pez-Moreno, and J. J. Laserna, Design, construction and assessment of a field-deployable laser-induced breakdown spectrometer for remote elemental sensing, *Spectrochim. Acta B At. Spectrosc.* 61(1), 88 (2006)
39. B. Sallé, P. Mauchien, and S. Maurice, Laser-induced breakdown spectroscopy in open-path configuration for the analysis of distant objects, *Spectrochim. Acta B At. Spectrosc.* 62(8), 739 (2007)
40. L. F. Qi, L. X. Sun, Y. Xin, Z. B. Cong, Y. Li, and H. B. Yu, Application of stand-off double-pulse laser-induced breakdown spectroscopy in elemental analysis of magnesium alloy, *Plasma Sci. Technol.* 17(8), 676 (2015)